nature communications

Article

https://doi.org/10.1038/s41467-024-51481-9

Fallopian tube rheology regulates epithelial cell differentiation and function to enhance cilia formation and coordination

Received: 14 June 2023

Accepted: 8 August 2024

Published online: 28 August 2024

Check for updates

Melati S. Abdul Halim[1], Jennifer M. Dyson[2,3], Max M. Gong[4], Moira K. O'Bryan[5] & Reza Nosrati[1]

The rheological properties of the extracellular fluid in the female reproductive tract vary spatiotemporally, however, the effect on the behaviour of epithelial cells that line the tract is unexplored. Here, we reveal that epithelial cells respond to the elevated viscosity of culture media by modulating their development and functionality to enhance cilia formation and coordination. Specifically, ciliation increases by 4-fold and cilia beating frequency decreases by 30% when cells are cultured at 100 mPa·s. Further, cilia manifest a coordinated beating pattern that can facilitate the formation of metachronal waves. At the cellular level, viscous loading activates the TRPV4 channel in the epithelial cells to increase intracellular Ca^{2+}, subsequently decreasing the mitochondrial membrane potential level for ATP production to maintain cell viability and function. Our findings provide additional insights into the role of elevated tubal fluid viscosity in promoting ciliation and coordinating their beating—a potential mechanism to facilitate the transport of egg and embryo, suggesting possible therapeutic opportunities for infertility treatment.

The female reproductive tract is a complex microenvironment lined with folded epithelium that provides a range of rheological and biochemical cues to facilitate fertilisation[1–3]. The geometrical complexity of the tract, including epithelial folds and crypts, considerably increases surface area to enhance nutrient transport, optimising the environment for egg support and fertilisation[4,5]. The tubal fluid in the fallopian tube originates from blood plasma transduction[6] and secretion of metabolic components and proteins via the lining epithelium[7,8]. The secretory products such as glucose, amino acids and oviduct-specific glycoprotein play important roles in reproductive events[9] by providing nutrients to promote gamete function and embryo development[10]. Steroid hormones, such as progesterone and oestrogen, regulate the secretory activity of epithelial cells to modulate the composition and concentration of their secretions, thus altering the rheology of the tubal fluid[11–13]. The epithelium lining the tract becomes less extensively folded and decreases in height from the ampulla to the isthmus[14], coupled with an increasing depth of crypts[15]. During the menstrual cycle, crypt epithelium consists mainly of secretory cells[15]. Hence, the viscosity of the mammalian tubal fluid varies considerably along the fallopian tube[16,17], radially (near the folds, crypts and lumen) and throughout the menstrual cycle[18,19], ranging from 1 mPa·s (similar to that of water) to over 10^3 mPa·s (similar to that of glycerine)[19–23]. The tubal fluid is more viscous at the utero-tubal junction—the port of entry to the fallopian tube[6] and decreases towards the ampulla and infundibulum at the distal end[7,9]—a mechanism to prevent sperm with poor motility from entering the fallopian tube[24,25]. The composition of oviductal secretion also varied over the menstrual cycle, induced by endocrine stimuli and influenced by both paracrine and autocrine effects[26]. The tubal fluid is most viscous at the pre-ovulatory stage and gradually decreases post-ovulation[14,27,28] to facilitate fertilisation by

[1]Department of Mechanical and Aerospace Engineering, Monash University, Clayton, Victoria, Australia. [2]Department of Materials Science and Engineering, Monash University, Clayton, Victoria, Australia. [3]Department of Biochemistry and Molecular Biology, Biomedicine Discovery Institute, Monash University, Clayton, Victoria, Australia. [4]Department of Biomedical Engineering, Trine University, Angola, IN, USA. [5]School of BioSciences and Bio21 Molecular Science and Biotechnology Institute, Faculty of Science, University of Melbourne, Parkville, Victoria, Australia. e-mail: Reza.Nosrati@monash.edu

accentuating sperm flagellar beat dynamics[23,29] and progression of sperm towards the egg[14,30]. While most focus has been on exploring the effects of viscosity on sperm swimming behaviour[31–33], the role of such a complex and dynamic rheological environment on the differentiation and function of epithelial cells within the female reproductive tract is unknown.

Fallopian tube epithelial cells (FTEC) include secretory and ciliated cells[34,35]. Secretory cells function to nourish gametes and embryos, while ciliated cells with actively beating cilia[36,37] regulate the flow and form metachronal waves[38] to transport the egg and embryo along the tube[34,39,40]. The ratio of ciliated to secretory cells changes during the menstrual cycle[39,41] and also increases along the length of the fallopian tube, from ~30% in the isthmus to ~80% closer to the site of fertilisation in the ampulla[34,42]. Defects in cilia formation, function or the cooperative cilia beating behaviour (with either sperm or egg) can result in infertility[43,44]. A three-dimensional (3D) cellular microenvironment has been shown to be crucial for the development of epithelial cells, as ciliated cells rapidly transform into flattened cells without cilia in a two-dimensional (2D) culture system[45,46]. However, the role of viscosity in the formation and differentiation of ciliated and secretory epithelial cells is unknown. Similar mechanical and physical stimuli in the extracellular environment have been shown to influence the development and function of other cell types[47–50]. The viscoelasticity and crosslinking density of extracellular fluid (ECF) influence the spreading behaviour of breast cancer cells, liver cancer cells and fibroblast by activating their mechanotransductive signalling pathways[51–53]. This additional mechanical loading due to an increase in the viscosity causes actin remodelling, cell swelling and calcium influx regulation via the transient receptor potential vanilloid 4 (TRPV4) channel in breast and brain cancer cells[52,54], leading to increased cell contractility and collectively enhancing cell migration. The activation of TRPV4 channel on oviductal ciliated cells by inducing viscous loading over just 10 min also regulates the ciliary beating frequency and elevates intracellular Ca^{2+} levels[55]. Similar mechanical and rheological stimuli regulate sperm swimming behaviour near flat or curved surfaces and at higher viscosities[14,56] and have provided unique microfluidic opportunities to select high-quality sperm in high-viscosity media[57,58], demonstrating the importance of probing the effects of extracellular fluid viscosity for a better understanding of the event of fertilisation.

Traditional static cell culture models have been used to understand the biophysics and biomolecular mechanisms of cellular functions, due to the possibility of controlling the growth environment and maintaining cell homogeneity in vitro[59]. Recently, microfluidic organ-on-a-chip systems have offered new capabilities to closely mimic the in vivo microenvironment compared to conventional cell culture platforms[60,61]. Biological organs such as the liver, lung, brain and skin were reconstructed in organotypic micro-platforms ex vivo such that they are able to reproduce their natural form and function[62,63]. In the context of mammalian reproduction, microfluidic culture models of the fallopian tube have been shown to be able to recapitulate the human 28-day menstrual cycle hormone profile[64] and improve bovine embryo production[65]. These organotypic platforms demonstrate the involvement of epithelial cells in the programming of an early embryo genome for improved implantation rates[66] and their secretions help to reduce parthenogenic oocyte activation[65]. While these culture models advanced our understanding of cellular and molecular processes relevant to mammalian reproduction, the role of tubal fluid viscosity on the differentiation and function of FTEC has not been addressed to date.

Here, by elevating the culture media viscosity to mimic the rheological properties of the fallopian tube tubal fluid[19], we explore the effects of mechanical stimuli on FTEC differentiation and functionality. Our findings reveal that an increase in the culture media viscosity from 1 mPa·s to 200 mPa·s regulates cell proliferation, reduces cell count, and significantly enhances ciliation by 4-fold. This is potentially attributed to a mechanistic response of FTEC, possibly via activation of the yes-associated protein (YAP) transcription factor to inhibit the Notch signalling pathway. Most notably, FTEC cultured in elevated viscosity also demonstrate a 30% reduction in cilia beating frequency but self-organise to facilitate the formation of metachronal waves. By blocking relevant ion channels in controlled experiments, we demonstrate that FTEC elevate intracellular Ca^{2+} level via TRPV4 channel in response to viscous loading, and subsequently, increase their mitochondria activity for adenosine triphosphate (ATP) production to maintain their viability and functionality. Collectively, our findings provide additional insights into understanding the biology of reproduction and the crucial role of tubal fluid viscosity in promoting ciliation and coordinated cilia beating to facilitate fertilisation.

Results

Viscous loading enhances the proportion of ciliated epithelial cells

To simulate a physiologically relevant range of ECF viscosity[19,21], we cultured epithelial cells in media supplemented with 0%, 0.7%, 0.82% and 1% methylcellulose (MC, see "Methods"), representing culture media with nominal viscosities of 1 mPa·s, 50 mPa·s, 100 mPa·s and 200 mPa·s, respectively. To facilitate cell attachment and ensure a valid comparison, we first seeded the cells at 8×10^5 cells per well on collagen-coated plates using 1 mPa·s culture media (0% MC) for 24 h (Fig. 1a). This resulted in a similar number of cells attached per well and similar confluency levels before switching to culture media of varying viscosities. Upon cell attachment, we then cultured the cells in media of different viscosities for another 48 h, replacing the media every 24 h. While the number and viability of aspirated cells remained similar (Supplementary Fig. 1), the confluency of cultured cells decreased considerably by increasing the media viscosity at the 72-h time point (Fig. 1a). Specifically, the 1 mPa·s culture demonstrated a high level of confluency, but the confluency level decreased by approximately 54% at 200 mPa·s (Fig. 1a).

Cell density (number of cells per unit area of the well) also decreased significantly from $2.1 \pm 0.1 \times 10^5$ cells/cm^2 to $0.9 \pm 0.1 \times 10^5$ cells/cm^2 by increasing the culture media viscosity from 1 mPa·s to 200 mPa·s (Fig. 1b, c; Methods). However, the area covered by each cell increased from 431 ± 139 μm^2 to 1052 ± 356 μm^2 by increasing the culture media viscosity from 1 mPa·s to 200 mPa·s (Fig. 1d). This indicates that increased fluid viscosity encourages cell spreading, as also reported for human liver cancer cells under viscous loading[51]. Interestingly, despite a lower overall cell count, the proportion of ciliated cells increased considerably by 4-fold (from $2.7 \pm 0.9\%$ to $10.0 \pm 1.8\%$, Fig. 1b, e) by increasing media viscosity from 1 to over 100 mPa·s. This reveals the influence of media viscosity on epithelial cells ciliation, despite a lower preference for attachment to plates by ciliated cells compared to secretory cells[45,67]. We also measured the osmolarity of the culture media (Supplementary Table 1, see "Methods"), which decreased from 312 mOsm/kg at 1 mPa·s (0% MC) to 257 mOsm/kg at 200 mPa·s (1% MC), within the physiologically relevant range of osmolarity for oviductal fluid in mammals and embryo culture media (ranging from 250 to over 355 mOsm/kg)[68,69]. This change in osmolarity might also contribute to the effects observed here. Our results demonstrate the role of mechanical stimulation via viscous loading in regulating epithelial cell differentiation and ciliation. During the menstrual cycle, secretory cells regulate the viscosity of the in vivo fluid by changing the protein content and composition of the tubal fluid[70]. This change in viscosity may contribute as a natural mechanism to trigger ciliation.

We also compared our well plate culture system with cells cultured in transwell systems under different viscosities (Supplementary Fig. 2). For cell culture using transwell systems, the same overall trend as in traditional well plates was observed, where the proportion of

https://doi.org/10.1038/s41467-024-51481-9

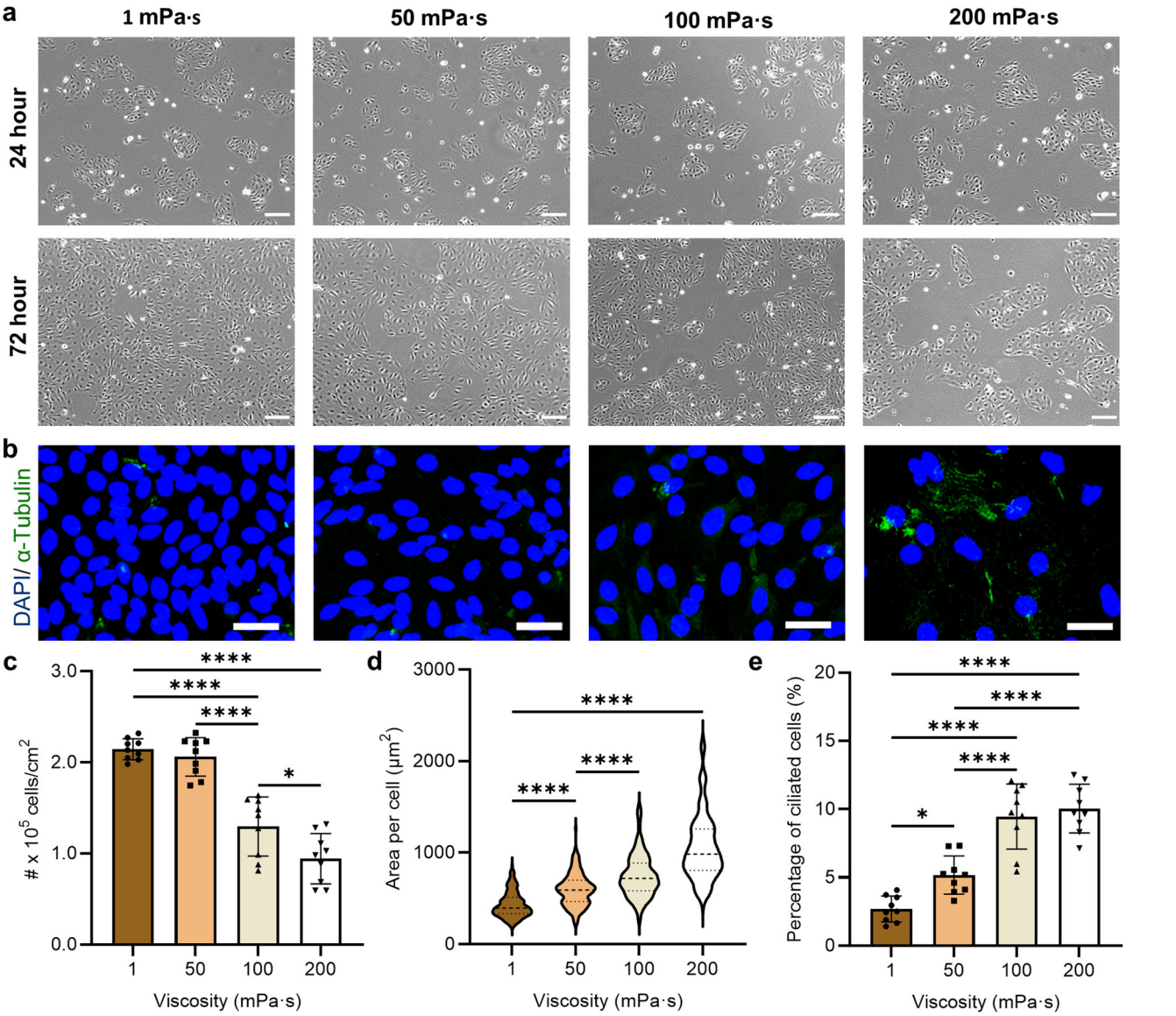

Fig. 1 | Effect of culture media viscosity on the development of the fallopian tube epithelial cells (FTEC). a Representative phase contrast images of FTEC 24 h (top) and 72 h (bottom) post-seeding as a function of culture media viscosity ranging from 1 mPa·s to 200 mPa·s. **b** Representative immunofluorescent images of FTEC 72 h post-seeding, where the green stain indicates the cilia and the blue stain indicates nuclei. Scale bars, 30 μm. **c** Epithelial cell density (number of cells per cm^2, $n = 9$ images from three biological replicates per each condition), **d** area per cell ($n \geq 200$ single cells from three biological replicates per each condition), and **e** the proportion of ciliated cells as a function of viscosity ($n = 9$ images from three biological replicates per each condition), after 72 h of culture. Data are represented as mean ± s.d. and analysed using one-way ANOVA with Tukey post hoc testing, $^{*}P \leq 0.05$, $^{**}P \leq 0.01$, $^{***}P \leq 0.001$ and $^{****}P \leq 0.0001$. For exact P values see Supplementary Table 3. Source data are provided as a Source Data File.

ciliated cells increased significantly with increasing media viscosity (from 6.5% at 1 mPa·s to 18.5% at 200 mPa·s). These results indicate that high-viscosity culture also facilitates ciliation in epithelial cells. Moreover, the overall morphology of the cells was comparable between well plate and transwell systems (Supplementary Fig. 2c), with no significant changes in cilia length ($P \geq 0.05$) between the two culture systems (well plate vs. transwell). Both measurements were also directly comparable with the cilia length of cells from the epithelial tissue (4.9 ± 0.3 μm). Interestingly, the percentage of ciliated cells under transwell culture was higher compared to cells in a well plate. This lower percentage of ciliated cells in well plates is potentially attributed to the inherent nature of our 2D culture system, which promotes flattening and deciliation of epithelial cells[45,46]. In contrast, the viscoelastic and inherent 3D structure of MC polymeric chains in high-viscosity buffers may have the opposite effect, facilitating ciliation. This latter result is relevant to previous work where viscoelasticity and extracellular fluid density have been shown to influence the development and spreading behaviour of other cell types[51–53]. It is noteworthy that the cell density (number of cells per unit area of the well) of cells cultured in transwell maintained the same decreasing trend as compared with well plate culture, decreasing from $2.2 \pm 0.1 \times 10^5$ cells/cm^2 at 1 mPa·s to $1.6 \pm 0.1 \times 10^5$ cells/cm^2 at 200 mPa·s (Supplementary Fig. 2d), with no significant changes in nucleus size between well plate and transwell cultures (Supplementary Fig. 2e). This comparable trend and similar behaviour of cells in the well plate and transwell systems suggest the role of high-viscosity fluidic environments in maintaining the developmental behaviour of ciliated epithelial cells, hindering their rapid dedifferentiation into secretory cells as traditional well plate culture systems at low viscosities do.

https://doi.org/10.1038/s41467-024-51481-9

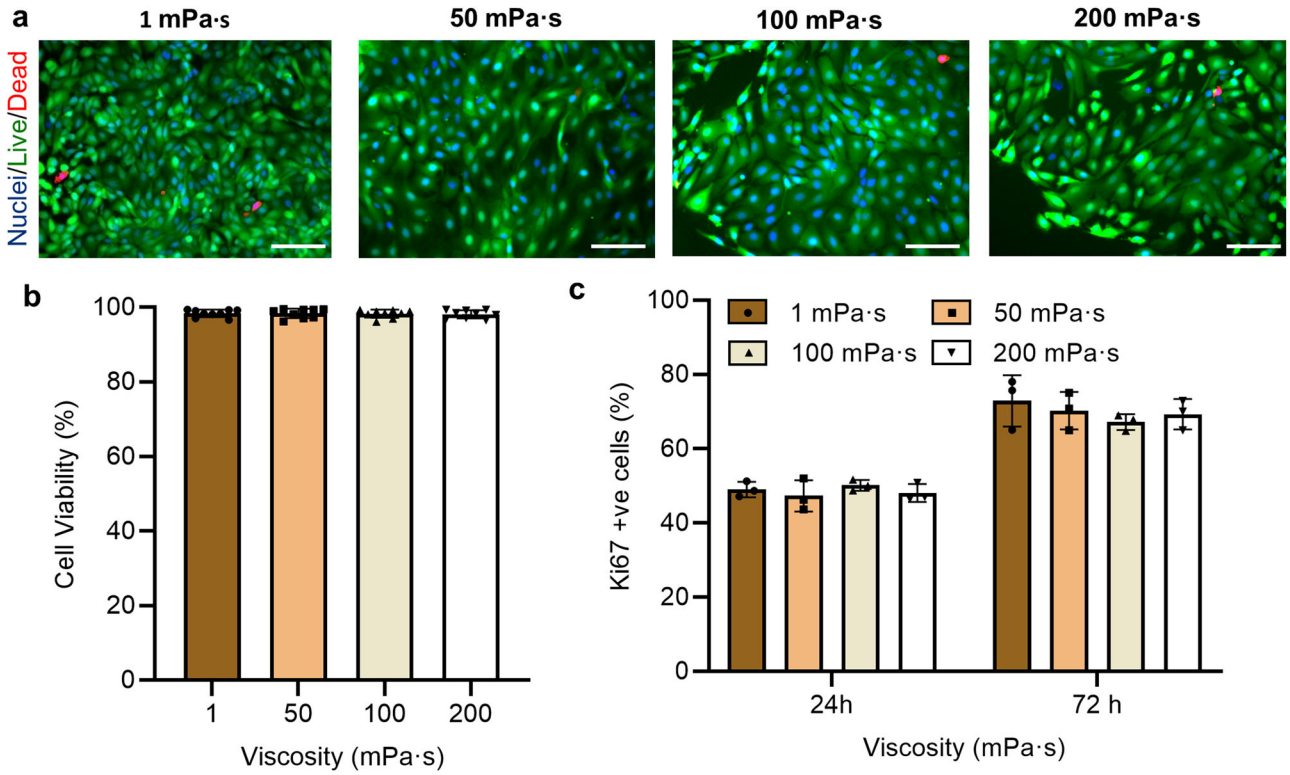

Fig. 2 | Effect of culture media viscosity on FTEC viability and proliferation. **a** Representative live/dead (green/red) fluorescence staining images of cells at the 72-h time point and the **b** percentage of live cells (cell viability). Cell nuclei were stained using blue-fluorescent Hoechst 33342 ($n = 9$ images from three biological replicates per each condition). Scale bar, 50 μm. **c** The percentage of Ki-67 positive cells at the 24-h and 72-h time points. Experiments were carried out on $n = 3$ from three biological replicates and ≥ 200 cells for each condition were analysed. All data are represented as mean ± s.d. and analysed using one-way ANOVA with Tukey post hoc testing. Source data are provided as a Source Data File.

To evaluate the role of viscosity on cell viability, as a potential cytotoxic factor to affect cell counts, we stained the cells at the 24-h and 72-h time points with green-fluorescent calcein-AM and red-fluorescent ethidium homodimer-1 to indicate live and dead cells, respectively (Fig. 2a, see "Methods"). At each time point, the cells maintained a consistent viability of ~90% regardless of the culture condition (Fig. 2b), demonstrating no cytotoxic effects in response to viscous loading. Ki67 staining was also used to assess whether the change in cell count was a consequence of a change in proliferation (Fig. 2c). While we observed a ~ 55 % increase between the 24-h and 72-h time points (from an average of 42 % to 65 %), no significant change in proliferation was detected in response to viscous loading at each time point (Fig. 2c). We also evaluated the number of dead cells being aspirated from the culture as we replaced the media between different time points, and similarly no significant change was observed between different culture conditions (Supplementary Fig. 1). Considering the lower cell counts (Fig. 1c) and higher proportion of ciliated cells (Fig. 1e) at higher viscosities, the results suggest that viscous loading enhances the proportion of cells that are differentiating into ciliated cell, independent of the proliferation rate.

Proliferation of FTEC under viscous loading over multiple passages

FTEC, particularly ciliated cells, are often sourced from primary cultures, where cells are dissociated from fresh tissue, due to challenges associated with maintaining viability and ciliation over multiple passages[45,71]. To indicate the proliferation competency of cells over time, Fig. 3 compares the percentage of actively proliferating cells (Ki67 positive cells) over 3 passages (a total of 9 days) as a function of viscosity. The proliferative capability of cells after 1 and 3 passages were comparable ($P \geq 0.05$, ANOVA followed by a post hoc Tukey test) for cells cultured in 1 mPa·s, 50 mPa·s and 200 mPa·s, with a slight decrease from 69 ± 2% to 65 ± 3% ($P < 0.05$, ANOVA followed by a post hoc Tukey test) for cells cultured in 100 mPa·s (Supplementary Table 2). Moreover, the percentage of proliferating cells rate was similar for passage 1 cells, regardless of media viscosity, with a higher proportion of ciliated cells at higher viscosities (similar to results shown in Fig. 1e). However, after 3 passages, the percentage of Ki67 positive cells decreased by 9% (from 74% to 65%) by increasing the media viscosity from 1 mPa·s to 100 mPa·s, and then increased back to 72% for cells cultured at 200 mPa·s. While the cells demonstrated active proliferation by mitosis over multiple passages, the results suggest the potential role of high viscous loading on maintaining growth and differentiation competency of the FTEC over time.

Viscous loading facilitates self-organisation and coordination of ciliated cells

The dominant factors of ciliary transport are the beating frequency and direction which can be regulated by chemical and mechanical cues[72] to form metachronal waves for transporting egg and embryo along the fallopian tube[34,39,40]. To quantitatively analyse cilia beating behaviour at different viscosities, a fast Fourier transform algorithm, based on a model developed by Ringers et al.[73] (Supplementary Fig. 3, see "Methods"), was used to evaluate cilia beating and coherence as a measure of cilia coordination. In this model, a frequency map was established by grouping cells with similar oscillation frequencies (± 0.5 Hz) into patches (Supplementary Fig. 4). Figure 4 compares the dynamic properties of cilia beating and coordination of cells cultured at different viscosities (Supplementary Movie 1). When comparing phase angles (as an indicator of the phase difference between neighbouring patches), larger areas with relatively similar phase angles were observed at lower viscosities (as suggested by the colour map in

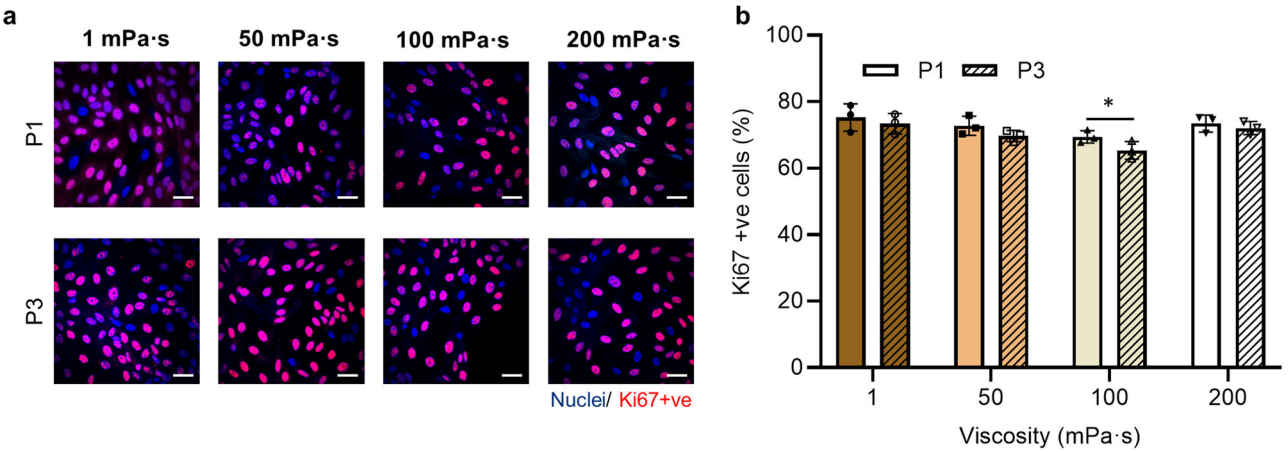

Fig. 3 | Comparison of FTEC proliferation between the initial culture and after 3 passages as a function of viscosity at 72-hour time point for each passage. **a** Representative Ki67 positive staining images of cells at the 72-h time point for passages 1 and 3, and the **b** percentage Ki67 positive cells. Scale bar, 30 μm. Experiments were carried out on $n = 3$ from three biological replicates and ≥ 200 cells for each condition were analysed. Data are represented as mean ± s.d. and analysed using a two-tailed t-test, $^*P \le 0.05$ ($P = 0.0131$). Source data are provided as a Source Data File.

Fig. 4b) with an average standard deviation of 1.2 rad and 1.1 rad between neighbouring patches at 1 mPa·s and 50 mPa·s, respectively (Supplementary Fig. 5). However, as the culture viscosity increased to 100 mPa·s and 200 mPa·s, smaller areas with a similar phase angle and a smooth transition between neighbouring areas were observed, with an average standard deviation of 1.3 rad and 1.7 rad, respectively (Supplementary Fig. 5). The results reveal viscous loading induces a phase shift between neighbouring cilia, that is crucial to the development of metachronal waves[74,75]. Interestingly and in contrast to the phase angle results, the wave direction (Fig. 4c, Supplementary Fig. 6) and wavelength (Fig. 4d, Supplementary Fig. 7) were relatively similar between neighbouring patches of cells cultured at higher viscosities. At 200 mPa·s in particular, a relatively stable wave direction (Fig. 4c) and a significantly larger ciliated area ($P \le 0.01$, Supplementary Fig. 8) with a similar wavelength of 2.13 ± 0.74 μm was observed. To better evaluate how this coordinated cilia movement might facilitate the formation of metachronal waves or enable effective transport, we manually traced cilia beating direction and used kymographs as the common approach[73,76] to evaluate whether the metachronal wave-like activity was present (Supplementary Fig. 9, Supplementary Movie 2). While cilia beat randomly relative to each other at 1 mPa·s, our results indicate that cilia not only coordinate in phase but also in direction, beating in a coordinated manner towards one direction at 200 mPa·s. Our kymograph results (Supplementary Fig. 9b) also show how cilia movement results in a smooth wave with a stable direction over time at high viscosity, suggesting the formation of metachronal waves.

The average cilia beating frequency decreased significantly by 30% (from 13.3 ± 1.2 Hz to 9.1 ± 0.7 Hz, $P \le 0.0001$) by increasing the culture media viscosity from 1 mPa·s to 50 mPa·s, and then plateaued at 7.9 ± 0.5 Hz ($P \ge 0.05$) at higher viscosities (Fig. 4e). To test the hypothesis that TRPV4 channel contributes to maintaining cilia beating frequency at higher viscosities, we repeated our experiments in the presence of the TRPV4 antagonist RN-1734 (see "Methods"). At 200 mPa·s, the cilia beating frequency further decreased to 5.3 ± 0.5 Hz for cells treated with RN-1734 (Fig. 4e), while the results for the vehicle control were comparable to untreated cells. The results indicate that ciliary beating is sustained at high viscosity through the activation of TRPV4 channels, which subsequently increase the intracellular calcium level. To further quantify the collective beating behaviour of ciliated cells, Fig. 4f shows coherency as a function of culture media viscosity (see "Methods"). The coherence level significantly increased by 102% (from 1443 ± 380 to 2919 ± 681) when the viscosity of the culture media increased from 1 mPa·s to 200 mPa·s ($P \le 0.0001$), indicating the effects of mechanical stimulation caused by the viscous loading on cilia coordination and the overall beating consistency. In contrast, cells treated with RN-1734 to block the TRPV4 channel exhibited a considerably lower coherence level at 200 mPa·s (Fig. 4f), highlighting the role of this channel in regulating cilia beating and coordination. These results align with previous studies that used a TRPV4 activator to demonstrate that TRPV4 regulates ciliary beating in both oviduct ciliated cells and tracheal cilia at high viscosities[55,77], further supporting the role of TRPV4 in ciliary activity regulation. These results indicate that, under viscous loading, ciliated cells self-organise their beating behaviour to form waves of similar frequency, direction and wavelength, associated with a shift in phase angle over a relatively large area to facilitate the formation of metachronal waves.

TRPV4 expression is regulated in response to viscous loading

TRPV4 channel is a calcium-permeable cation channel that is sensitive to osmotic and mechanical stimulation[78,79]. To assess the role of the TRPV4 channel in regulating intracellular calcium levels, we monitored calcium uptake over a period of 120 s for cells treated with RN-1734 (to block the TRPV4 channel) as compared with a control group of vehicle-treated cells (Fig. 5a, see "Methods"). Calcium uptake was reduced by up to 40% in cells with blocked TRPV4 channels, indicating the crucial role of this channel in modulating calcium influx into the cytosol in response to viscous loading. In non-blocked cells, increase in intracellular Ca^{2+} level elevates the influx of cytosolic Ca^{2+} into the mitochondria[80,81], reducing the mitochondrial membrane potential (MMP)[82,83] and increasing ATP production[84–86]. To test the cellular response under viscous loading, cultured FTEC were stained with JC-1 dye to evaluate the MMP level (Fig. 5b–d). JC-1 dye exhibits a potential-dependent accumulation in mitochondria such that low MMP cells with JC-1 monomer emit green fluorescence and high MMP cells with JC-1 aggregate emit red fluorescence (Fig. 5b, c). Consequently, mitochondrial depolarization can be indicated by an increase in the ratio of cells with low MMP to high MMP[87] (see "Methods"). As shown in Fig. 5d, our results demonstrate a 38% increase in the low MMP/high MMP ratio (from 0.13 ± 0.02 to 0.18 ± 0.02) by increasing the culture viscosity from 50 to 100 mPa·s ($^*P \le 0.05$; ANOVA followed by a post hoc Tukey test).

To evaluate ATP production, cells cultured in different viscosities were also stained using MitoTracker deep red (Supplementary Fig. 10, see "Methods") that specifically labels respiring mitochondria[88]. Epithelial cells cultured at higher viscosities showed a significantly higher level of mitochondrial respiration (63% increase when comparing

https://doi.org/10.1038/s41467-024-51481-9

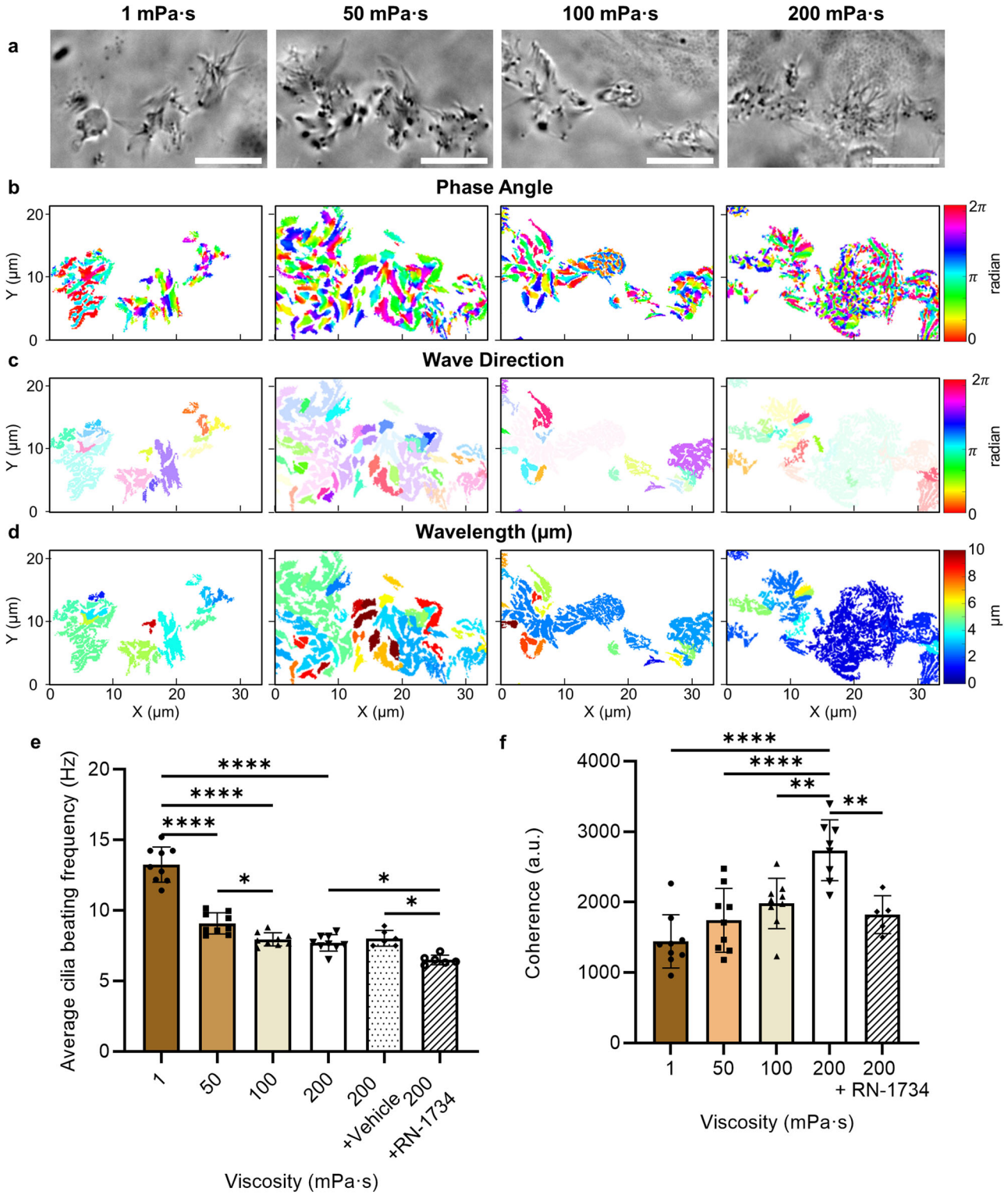

Fig. 4 | Characterisation of cilia beating and coordination under viscous loading. a Representative widefield images of live ciliated cells, and the corresponding (**b**) phase angle, (**c**) wave direction and (**d**) wavelength of beating cilia as a function of media viscosity. Scale bars, 10 μm. **e** Average cilia beating frequency, and **f** coherence (a measure of the cilia coordination) as a function of culture media viscosity and for cells treated with RN-1734 to block the TRPV4 channel, and for the vehicle control. Data are represented as mean ± s.d. and analysed using one-way ANOVA with Tukey post hoc testing, $^{*}P \le 0.05$, $^{**}P \le 0.01$ and $^{****}P \le 0.0001$, $n = 9$ images from three biological replicates per each condition. For exact P values see Supplementary Table 3. Source data are provided as a Source Data File.

cultured cells at 1 mPa·s with 200 mPa·s), indicating that more mitochondria are respiring under viscous loading to convert the intracellular energy to ATP. The results also agree with previous findings where a decrease in MMP increases mitochondria ATP production[84–86].

To further elucidate the effects of viscosity on TRPV4 activity, we evaluated the expression of TRPV4 using a TRPV4 antibody (see "Methods")[89]. A linear rise in TRPV4 intensity ($R^2 = 0.99$) was observed, with a 5-fold increase in intensity (i.e. active TRPV4 channels) when the

https://doi.org/10.1038/s41467-024-51481-9

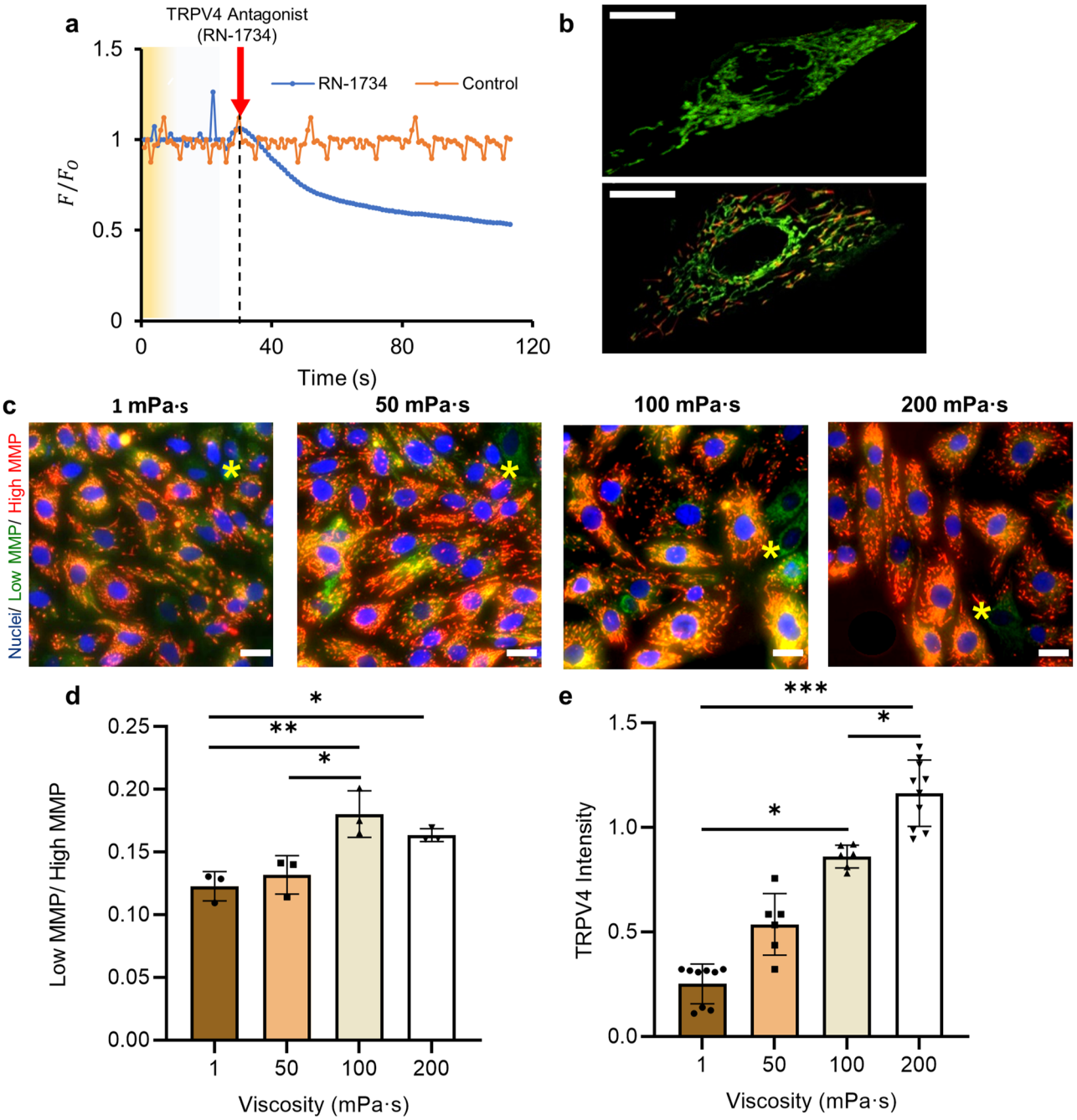

Fig. 5 | Effects of viscous loading on intracellular calcium uptake, mitochondrial membrane potential and TRPV4 expression. a Calcium uptake expressed as the ratio of F/F_0 over 120 s for cells treated with control or RN-1734 (to block the TRPV4 channel) as compared with a control group of untreated cells. F is the instantaneous fluorescence intensity and F_0 is the baseline intensity. **b** The zoomed-in view for a low MMP cell with JC-1 monomer (top) and a high MMP cell with JC-1 aggregate (bottom). Scale bar, 10 μm. **c** Representative overlaid immunofluorescence staining images of epithelial cells stained with JC-1 at 72-h time point as a function of culture media viscosity. JC-1 monomers and aggregates were imaged in green and red channels, respectively. The asterisks (*) indicate cells with low mitochondrial membrane potential (MMP). Cell nuclei were stained using blue-fluorescent Hoechst 33342. Scale bar, 20 μm. **d** The ratio of low MMP (green) to high MMP (red) cells as a function of culture media viscosity, indicating the degree of depolarization. Experiments were carried out on $n = 3$ from three biological replicates and ≥ 200 cells for each condition were analysed. **e** TRPV4 fluorescence intensity (TRPV4 activated channels) in cells as a function of culture media viscosity, $n \geq 6$ images from three biological replicates per each condition. All data are represented as mean ± s.d. and analysed using one-way ANOVA with Tukey post hoc testing, $^*P \leq 0.05$, $^{**}P \leq 0.01$, $^{***}P \leq 0.001$. For exact P values see Supplementary Table 3. Source data are provided as a Source Data File.

culture viscosity was elevated from 1 to 200 mPa·s (Fig. 5e, Supplementary Fig. 11). It is noteworthy that, while TRPV4 is an ion channel, it can be immunolocalised at the cytoplasm due to the potential trafficking pathways of the ion channel to and from the plasma membrane, as confirmed by previous studies using the same immunofluorescent staining antibodies[89–91]. Since TRPV4 channels can also be activated via agonists such as phorbol ester (4α-PDD) and GSK1016790A, Baratchi et al.[90] reported that GSK1016790A induces the translocation of TRPV4 from the plasma membrane to the cytoplasm, where the channels formed vesicular structures with concentration-dependent cytoplasmic aggregation. Differentiated mouse mammary epithelial cells (HC11) cultured in a growth medium also demonstrated TRPV4 protein pooled in intracellular cytoplasmic compartments for both single and clustered cells[92].

We also compared TRPV4 expression for cells at different viscosities using Western blot (see "Methods"). TRPV4 protein expression increased under high-viscosity conditions (Supplementary Fig. 12), specifically by about 1.5-fold when media viscosity increased from 1 mPa·s to 200 mPa·s. This is supported by our calcium uptake results (Fig. 5a), showing that inhibition of TRPV4 with RN-1734, a well-established TRPV4 channel inhibitor[93], leads to a significant reduction in calcium influx into the cell. Overall, our results indicate that viscous loading leads to increased TRPV4 expression and encourages ciliation. Conversely, blocking TRPV4 channel restricts cilia beating frequency and coherence (Fig. 4e, f), consistent with similar previous work including those that used knockout mouse models[52,77]. Therefore, viscous loading activates TRPV4 channel to increase intracellular Ca^{2+}, subsequently decreasing the MMP level and increasing ATP production to maintain cell viability and functionality at higher viscosities.

Discussion

We used culture media viscosity mimicking the rheological properties of the fallopian tube[19] to study the effects of mechanical stimuli on FTEC differentiation and function. Our results reveal that increasing extracellular fluid viscosity from 1 mPa·s to 200 mPa·s significantly enhances the proportion of ciliated cells by 4-fold while reducing cell density by 57%. This increase in viscosity orchestrated cellular differentiation, as the cells also exhibited active proliferation and maintained high cell viability (~ 90%) after 72 h of culture. These findings suggest that viscous loading can regulate ciliation by enhancing the proportion of cells that are differentiating into ciliated cells, independent of the proliferation rate. It is noteworthy that a slight change in the osmolarity of culture media, within the physiologically relevant range (from 312 mOsm/kg to 257 mOsm/kg, Supplementary Table 1), due to the increasing MC concentration, might also contribute to the regulation of epithelial cell behaviour. While considerably more significant changes in osmolarity have been reported to regulate airway epithelial cells behaviour and cilia length[94], this effect is potentially negligible here as we do not see changes in cilia length (Supplementary Fig. 2). Previous studies using up to 2% MC or 1% Dextran (with similar osmolarity to 1% MC) have also shown insignificant changes in cell behaviour due to this range of changes in osmolarity[53].

The significant increase in ciliation at higher viscosities (Fig. 1e), with comparable trends between the well plate and transwell systems (Supplementary Fig. 2), and cilia lengths from these systems are similar to native tissue, indicate the crucial role of a high-viscosity environment in facilitating ciliation and maintaining the developmental behaviour of epithelial cells. This increasing ciliation trend is consistent with how the proportion of ciliated cells and viscosity change during the menstrual cycle as the epithelial tissue matures. Similar to our results, the ratio of ciliated to secretory cells increases during the menstrual cycle along with the tubal fluid viscosity, both peaking at the time of ovulation[27,95].

The activation of mechanosensitive transcription factors that inhibit the Notch signalling pathway in epithelial cells may serve as a potential mechanism to facilitate ciliation in response to viscous loading[34,96,97]. The Notch signalling pathway is a critical mediator of short-range cell-cell communication[97] that governs the fate of neighbouring cells, including cell proliferation, differentiation, and death. The inhibition of Notch signalling in a 3D organoid model of human fallopian tube[96] and embryonic epidermis of the amphibian *Xenopus laevis*[34] has been shown to regulate the balance between formation of ciliated and other cell types. YAP is a mechanotransductive transcription factor that can suppress the Notch signalling pathway[97], for example to promote cellular stemness in somatic stem cells[98] and endothelial cells[99]. YAP is responsible for sensing mechanical properties of the microenvironment[97], and is activated under elevated mechanical stresses[51,100]. Interestingly, extracellular fluid viscosity has also been shown to activate YAP in liver cancer cells (HepG2)[51]. Therefore, mechanoactivation of YAP under viscous loading can potentially suppress the Notch signalling pathway in epithelial cells to encourage ciliation and prevent cells from differentiating into secretory cells[34]. With respect to reproduction, these findings provide a foundation for future research into signalling pathways in healthy and diseased fallopian tubes, since one of the most common and important alteration in ovarian cancer patients is the deregulation of Notch signalling[101].

Moreover, our results indicate that viscous loading regulates the biophysics of cilia beating and coordination to potentially facilitate the formation of metachronal waves at higher viscosities (> 100 mPa·s). Specifically, the beating frequency of ciliated cells reduced significantly by over 30% by increasing culture viscosity, and plateaued at 7.9 ± 0.5 Hz for viscosities higher than 100 mPa·s. The combination of hydrodynamic effects, changes in ATP production rate, and potential regulation of the molecular motor activity that governs the movement of cilia may contribute to influence cilia beating behaviour at different viscosities[23,102,103]. The increased drag at higher viscosities can reduce the beating velocity of the cilia[104], and consequently their beating frequency. This increase in hydrodynamic resistance also leads to a decrease in cilia beating amplitude (Supplementary Fig. 13) and a higher energy consumption rate per beat cycle[23,103]. Moreover, similar to other flagellated eukaryotic cells, under viscous loading, the higher force production rate of dynein arms that govern the beating waveform may act as a molecular-level mechanism to regulate motor activity[105]. The higher Ca^{2+} influx and TRPV4 channel activity at higher viscosities, and the subsequent increase in ATP production, support this later mechanism.

At such high viscosities, ciliated cells also self-organised their beating behaviour to induce a phase shift between neighbouring cilia (Fig. 4b) while beating with a similar wave direction (Fig. 4c), cilia beating direction (Supplementary Fig. 9), wavelength (Fig. 4d), and frequency (Fig. 4e). This spatial heterogeneity in cilia beating (i.e. separate patches with a gradual phase shift), but with a similar beating frequency, wavelength and direction, is crucial to encourage the formation of metachronal waves[73,74], and has been shown to produce a unidirectional flow towards the uterus[106,107]. The coordinated movement of cilia to enable effective transport is further demonstrated by evaluating cilia beating direction and kymographs (Supplementary Fig. 9, Supplementary Movie 2). The results indicate that cilia self-organise to beat in a unidirectional manner with a stable wave direction over time at 200 mPa·s, while they beat randomly at 1 mPa·s. While our study is limited by the number of ciliated cells observed and our limited spatial resolution, this metachronal wave-like activity with unidirectional cilia movement under viscous loading can result in effective transport. The observed increase in the tendency of cilia to beat in the same direction has been shown to be an effective transport mechanism for airway epithelial cells[108,109], even in the absence of metachronal waves or beating coordination. This mechanism, together with fluid flow and muscle contractions[1,110], provides an effective means for the transport of the egg and embryo, which are up to 10 times larger than the cilia[111], at the time of ovulation when the viscosity peaks in vivo[19,112].

We also indicated that TRPV4 expression increases by 5-fold when the culture viscosity is elevated from 1 to 200 mPa·s (Fig. 5e). Since TRPV4 channels modulate calcium influx into the cytosol (Fig. 5a), this increase results in additional Ca^{2+} influx into the mitochondria[80,81], reducing the MMP ratio by 38% in response to viscous loading (Fig. 5c, d). This reduction in MMP leads to a 63% increase in mitochondrial respiration (Supplementary Fig. 10) and increases ATP production[84–86]. The increase in Ca^{2+} influx through the TRPV4 channel subsequently mediates cilia beating frequency (Fig. 4e), with cells treated with RN-1734 showing reduced cilia beating. Moreover, the higher influx of Ca^{2+} has been shown to sustain ciliary beating behaviour at high viscosities without collapse[55]. TPRV4 activity has also

been shown to regulate mechanotransduction via the YAP/TAZ nuclear-shutting mechanism in various cell types, such as cellular epithelial-mesenchymal transition (EMT) in keratinocytes, mesenchymal stem cells and HUVEC endothelial cells[113–115]. Hence, viscous loading activates the TRPV4 channel in FTEC to increase intracellular Ca^{2+}, possibly via the regulation of YAP, subsequently decreasing the MMP level and increasing ATP production to maintain cell viability and functionality at higher viscosities. Previous work has also demonstrated a correlation between TRPV4 expression and the menstrual cycle[116,117]. It has been shown that TRPV4 expression peaks at the time of ovulation[116], as does the tubal fluid viscosity[19,112], which is then downregulated post-ovulation as the progesterone level increases. The increase in progesterone level during the menstrual cycle has been suggested to suppress oviductal ciliation[118] and inhibit TRPV4 protein expression using mammary gland epithelial cells[117]. Therefore, our findings suggest how the interplay of changes in tubal fluid viscosity, progesterone level, and TRPV4 expression during the menstrual cycle might influence ciliation and cilia activity.

Our findings suggest that the interplay between TRPV4 expression levels and subsequent Ca^{2+} influx to increase ATP production is crucial for regulating cilia beating under viscous loading. When comparing cells with blocked TRPV4 channels to untreated cells (Fig. 4e, f), we observed a drop in cilia beating frequency and coherence, indicating that the reduction in ATP production due to lower Ca^{2+} influx[119,120] influences cilia beating. While ciliated cells can self-generate ATP through either oxidative phosphorylation in mitochondria or glycolysis within the cilium itself[121], the activation of relevant signalling pathways is required to achieve this. Hence, enhanced TRPV4 activity and mitochondrial function trigger more ATP production at higher viscosities to ensure persistent cilia activity. These findings are consistent with previous studies where ciliated cells incubated with TRPV4 ion channel activators (instead of inhibitors, as in our case) or ATP showed an increased cilia beating frequency[77], also confirming that additional ATP is required under increased viscous loading[122] to maintain cilia beating.

In the fallopian tube, viscosity varies from 1 mPa·s to over 200 mPa·s[19–22] along the tract, radially across the cross-section of the tract, and more importantly, throughout the menstrual cycle. These changes in the tubal fluid viscosity, combined with our findings, highlight the potential role of these rheological changes in altering sperm migration behaviour in vivo, coordinating the timing of fertilisation, and facilitating egg and embryo transport in the fallopian tube. The interactions between sperm and ciliated surfaces are suggested to provide storage sites for sperm[123,124], stimulate capacitation, and influence the timing of fertilisation[1,34]. Our findings suggest that increased viscosity of the tubal fluid, peaking at the time of ovulation[19,112], can enhance cilia beating and coordination to encourage metachronal wave formation. This enhanced cilia activity may act as a mechanism to release sperm from storage sites when they have gained fertilisation competence through direct physical contact with epithelial tissue[125], and also to coordinate this timing with egg transport in the tract for optimal meeting at the fertilisation site. Moreover, our findings are relevant to infertility cases where tubal flushing with oil-based media has been shown to significantly improve fertilisation outcomes, although the underlying mechanism of this fertility-enhancing effect has been unknown[126]. Our results suggest a potential mechanism for facilitating cilia beating and gametes transport within the reproductive tract due to an increase in tubal fluid viscosity from the introduction of oil-based media[126].

Taken together, our findings reveal that physiologically relevant changes in the viscosity of the tubal fluid regulate the differentiation and function of epithelial cells, via mechanotransductive signalling pathways. In the context of reproduction, our findings bring additional perspectives into the mechanistic response of FTEC to elevated tubal fluid viscosity that peaks during ovulation and along the reproductive tract to facilitate egg and embryo transport for successful fertilisation outcomes, with potential insights into embryo-endometrium layer interactions. This highlights the importance of matching the viscosity of tubal fluid in in vitro culture models to accurately replicate the natural developmental and functional properties of the epithelial cells, offering additional insights into studies of other tissues with ciliated epithelium. Our findings also offer additional insights into the underlying causes of infertility where abnormal changes in the tubal fluid viscosity can inhibit ciliation. Moreover, our approach suggests potential therapeutic opportunities for infertility or ovarian cancer patients, where viscous loading could be utilised to potentially rectify their deregulated Notch signalling pathway.

Methods

Viscous media preparation

Methyl cellulose (MC) is a water-soluble, non-ionic viscoelastic polymer that closely represents the rheological properties of the high viscosity ECF in the reproductive tract[19–22,53]. To prepare the viscosity-adjusted culture media, the Dulbecco's Modified Eagle Medium: Nutrient Mixture F-12 (DMEM/F-12) with no glutamine (ThermoFisher, 21331020) was supplemented with 0.7%, 0.8% and 1% MC (Sigma, M0512) in sterile conditions (corresponding to nominal viscosities of 50, 100 and 200 mPa·s, respectively). All culture media were also supplemented with 100 U mL^{-1} penicillin-streptomycin (Life technologies) and 10% (v/v) foetal bovine serum (FBS, Scientifix), and pH was adjusted to 7.4. The osmolarity of the culture media was measured using an osmometer (John Morris and Advanced Instruments, Model 2020) based on the manufacturer's guidelines.

Isolation of fallopian tube epithelial cells (FTEC)

Ewe oviducts were collected from the local abattoir (Wagstaff, Cranbourne) in cold phosphate-buffered saline (PBS) after slaughter and transported to the laboratory on ice. The abattoir (Wagstaff, Cranbourne) complies with the Australian animal welfare standards through annual audits conducted by AUS-MEAT Limited (Aus-Meat Limited Certificate of Accreditation Establishment No. 46, 578 & 2773). The isolation and cell seeding procedures were all done in a sterile condition and within 2 h of tissue collection. The oviducts were dissected free of surrounding tissue and washed three times in cold PBS. The oviduct was opened up and minced into smaller pieces. The cell dissociation process was done enzymatically in tubes with cold dissociation media[67]. Dissociation media were made up of Minimum Essential Medium (MEM, 11095080, ThermoFisher), supplemented with 1.4 mg ml^{-1} Pronase (Sigma-Aldrich, 10165921001) and 0.1 mg ml^{-1} DNAse (Sigma-Aldrich, DN25). The tubes were then rocked for 48 h at 4 °C. The dissociation media was then inactivated using 10% volume of FBS, and then centrifuged at 200 g for 5 min. The isolated cells were then resuspended in DMEM/F12 supplemented with 10% FBS and 1% penicillin-streptomycin (without any MC) for initial seeding.

Cell culture

Prior to seeding, 24-well plates were coated overnight with type IV collagen from human placenta (Sigma-Aldrich, C7521), and then rinsed three times with PBS. Cells were then seeded at $800{\times}10^3$ cells per well. Each culture was always maintained under humidified conditions at 37 °C with 5% CO_2. Upon cell attachment after 24 h, the media was replaced with the relevant viscosity-adjusted culture medium. The media was replaced at the 48-h time point and further analysis was carried out at 72-h timepoint. The same culture protocol was used for culturing cells in transwells, with cells seeded in the insert and the culture media in the bottom well replaced over time.

Quantification of cellular and nuclear phenotypes

To evaluate cell and nuclear phenotypes, phase contrast images (cell phenotypes) and Hoechst 33342 stained images (nuclear phenotypes)

were captured using an inverted IX83 fluorescence microscope (Olympus, Japan) equipped with an ORCA-Flash4.0 V3 Digital CMOS camera (Hamamatsu, Japan) and a 20× magnification objective (NA = 0.45) and the images were processed in ImageJ. Hoechst stained images were used to count the number of cells in each experiment.

Cell viability assay

Cell viability was assessed using a live/dead staining kit (L3224, Life Technologies) according to the manufacturer's instructions. Live/dead stain was conducted at both 24-h and 72-h time points. Images were taken using an inverted IX83 fluorescence microscope (Olympus, Japan) equipped with an ORCA-Flash4.0 V3 Digital CMOS camera (Hamamatsu, Japan) and a 20× magnification objective (NA = 0.45) and the quantitative analysis was performed using ImageJ. Cell viability was calculated as the percentage ratio of live cells to the total number of cells. At least 200 cells were analysed per measurement. The area covered per cell was quantified by manually tracing at least 200 individual cells in ImageJ for each condition for cells stained with Calcein AM.

Immunofluorescence Staining

To evaluate cell proliferation and ciliation alongside cell and nuclear morphology changes, immunofluorescence staining was performed. Cell monolayers were washed with PBS and fixed for 10 min in 4% paraformaldehyde (PFA, Sigma, USA) diluted in PBS at room temperature. Cells were washed three times in PBS (5 min per wash), permeabilized for 15 min with 0.2% Triton X-100 (Sigma, USA) diluted in PBS, and then blocked in 3% (w/v) bovine serum albumin (BSA) diluted in PBS for 30 min. Cells were then incubated in primary antibodies overnight at 4 °C, either with mouse anti-acetylated tubulin (Sigma, T7451, 1:10,000 dilution) for ciliation study, monoclonal mouse anti-Ki67 (Dako, M7240, 1:200 dilution) for proliferation study, or rabbit polyclonal TRPV4 antibody (Abcam, ab39260, 1:180 dilution) for TRPV4 assays. Cells were then washed three times in PBS (5 min per wash) and incubated for 1 h at room temperature with secondary antibodies Alexa Fluor 488 goat anti-mouse (Thermo Fisher Scientific, RS37120, 1:500 dilution in PBS) or with Rhodamine–conjugated goat anti-rabbit IgG (Proteintech, SA00007-2, 1:200 dilution) for TRPV4 assays. Nuclei staining was done by using Hoechst 33342 (ThermoFisher, 62249) diluted in Dulbecco's Phosphate Buffered Saline (DPBS, ThermoFisher, 14190144) at 5 $\mu g\,ml^{-1}$. Immunofluorescence staining microscopy images were captured using an Olympus FV3000 confocal microscope at 60× magnification (NA = 1.4, PLAPON oil immersion objective) for proliferation and ciliation study, and 100× magnification (NA = 1.4, UPLSAPO oil immersion objective) for TRPV4 assays, before being processed in ImageJ. Reconstructed confocal microscopy z-stacks were used to view the side profiles of ciliated cells and measure cilia length. The expression of TRPV4 channels in cultured cells was quantified using rabbit polyclonal TRPV4 antibody (Abcam, ab39260, 1:180 dilution) as the primary antibody and Rhodamine–conjugated goat anti-rabbit IgG (Proteintech, SA00007-2, 1:200 dilution) as the secondary antibody[89]. This primary antibody has been shown to specifically target TRPV4[89,90]. To ensure the secondary antibody does not result in nonspecific binding or autofluorescence, we also conducted a negative control experiment where the cells were only stained with the secondary antibody, resulting in no fluorescent signal (Supplementary Fig. 11). The average fluorescence was quantified using ImageJ (with background compensation) and expressed as arbitrary units. All immunofluorescence images for each antibody were acquired using identical parameters (HV, gain, offset) to ensure a consistent signal-to-noise ratio across datasets.

Mitochondrial membrane potential (MMP) measurements

JC-1 dye (Invitrogen, USA), was used to evaluate the MMP. JC-1 is a membrane-permeable dye that exhibits potential-dependent accumulation in mitochondria, emitting green fluorescence (~ 525 nm) in the monomeric form (low MMP) and red fluorescence (~ 590 nm) in aggregate form (high MMP). Briefly, 10 μM working solution of JC-1 was prepared by diluting 1.53 mM JC-1 stock solution in prewarmed DMEM/F-12 media. The cultured cells were rinsed with prewarmed the DMEM/F-12 solution, and then 200 μL of the JC-1 staining solution was added per well. The cells were incubated at 37 °C for 30 min in an incubator with 5% CO_2. An inverted IX83 fluorescence microscope (Olympus, Japan) equipped with an ORCA-Flash4.0 V3 Digital CMOS camera (Hamamatsu, Japan) and a 40× magnification objective (NA = 0.6) was used to image the stained cells in green and red fluorescence channels. To validate the JC-1 staining, 5 mM Carbonyl Cyanide Chlorophenylhydrazone (CCCP) was used as the MMP negative control to disrupt the membrane potential of JC-1 stained cells. Closed up view of the mitochondrial structure (Fig. 5b) was imaged using an Olympus FV3000 confocal microscope at 100× magnification (NA = 1.4, UPLSAPO oil immersion objective). To evaluate the degree of polarisation, the low MMP to high MMP ratio was quantified by counting the number of cells imaged in green (low MMP) and red (high MMP) fluorescent channels.

Mitochondria activity

MitoTracker® Deep Red (Invitrogen, M22425) was used to label mitochondria. Briefly, 1 mM stock solution is prepared by adding dimethylsulphoxide (DMSO). The stock solution was diluted to 200 nM working concentration using prewarmed Dulbecco's Modified Eagle Medium: Nutrient Mixture F-12 (DMEM/F-12, ThermoFisher, 21331020). Nuclei staining was done using Hoechst 33342 (ThermoFisher, 62249) at 5 $\mu g\,ml^{-1}$. Culture media was aspirated before the staining solution was added, and then the cells were incubated at 37 °C with 5% CO_2 for 30 min. Mitochondria activity was measured as the average fluorescence intensity per cell.

Cilia beating analysis

Cilia beating was analysed using a custom-written script in MATLAB, by modifying a code developed by Ringers et al.[73] to quantify beating frequency and coherence based on a fast Fourier transform method (Supplementary Figs. 3, 4). First, cilia beating across the viscosity range was recorded at 200 frames per second using a widefield Leica microscope equipped with a CMOS camera and a 100× magnification objective (NA = 1.4). The stacked images were spatially down-sampled by a factor of 5, and then Fourier transform of each pixel intensity over time was performed to obtain the cilia beating frequency. Noise (area without cilia movement) was removed using a 3×3 kernel, as reported by Ringers et al.[73], to identify regions with beating cilia. The neighbouring pixels with similar oscillation frequency (± 0.5 Hz) were then grouped into patches to establish cilia beat frequency map. The *angle()* function in MATLAB was used to extract the phase angle from the Fourier output, and the calculated phase angles were then used to quantify wave direction and wavelength using the *imgradienty(phase, 'prewitt')* function in MATLAB. The gradient map was generated over both x and y direction, and over phase and phase+π to adjust for the circular nature of the phase. From the gradient maps, wave directions and wavelengths were extracted as the mean angle and the mode magnitude per patch, respectively (Supplementary Figs. 6, 7). The coherence was expressed as the total area covered by ciliated cells (total area of the patches) over the number of segmented patches. To quantify cilia beating amplitude, the movement of the tip of the cilia in the top-view widefield microscopy videos was manually tracked in ImageJ, and the average maximum travelled distance over multiple cycles was reported. Cilia beating direction was evaluated for 750 ms and the wave propagation was analysed using the kymograph plugin in ImageJ. For TRPV4 inhibition experiment, cells were incubated with 10 μM of TRPV4 antagonist RN-1734 (Sigma-Aldrich, R0658) dissolved in DMSO prior to experiments. The inhibitor dissolved in DMSO for the 200 mPa·s media was used as the vehicle control.

Ca^{2+} transients imaging

The vehicle (DMSO) or RN-1734 treated cells were loaded with 5 μM Fluo-4, AM, (ThermoFisher, F14217) calcium indicator for ratiometric Ca^{2+} confocal imaging at the 72-h time point for 30 min at 37 °C. Cells were washed using Ca^{2+} free Hanks' Balanced Salt Solution (HBSS, Thermo Fisher Scientific, 14170112) according to the manufacturer's protocol before imaging. Cells were imaged continuously up to 120 s with an interval of 2 s on an Olympus FV3000 confocal microscope. Transient Ca^{2+} level was expressed as F/F_0, where F is the instantaneous fluorescence intensity and F_0 is the baseline intensity as calculated by averaging the fluorescence signal for the first 20 s.

Western Blot Analysis

Cell pellets were collected at the 72-h time point and lysed in Laemmli Sample Buffer (Bio-Rad). Samples were boiled at 95 °C for 5 min, then diluted and loaded into 10-well gels (Bio-Rad). The gels were run for 1 h, after which the protein was then transferred to a PVDF membrane (Immobilon®). The membrane was blocked in 5% non-fat milk for 1 h, then incubated with primary antibodies overnight (TRPV4, Abcam ab39260, GAPDH, Invitrogen, MA5-15738). Secondary antibodies against the primary (Goat Anti-Rabbit HRP conjugate, Invitrogen, 31460, and Goat Anti-Mouse HRP conjugate, Invitrogen, A16066) were incubated with the blot for 1 h. Blots were imaged using a Uvitec Chemiluminescence Imaging System and analysed with ImageJ. Two bands with molecular weights of ~98 kDa were detected, with the higher molecular weight band representing the glycosylated form[127,128], consistent with previous studies[129,130], confirming the expression of TRPV4. Protein expression for TRPV4 was normalised to GAPDH[131].

Statistics and Reproducibility

Each experiment was conducted using three independent biological samples with three repeats per biological sample, with ≥ 200 cells analysed per data point. No statistical methods were employed to predetermine the sample size, and no data were excluded from the analyses. Oviducts from different animals were randomly shipped by the abattoir and used in the study. GraphPad Prism version 8.0.2 (GraphPad Software, San Diego, CA, USA) was used to process data. A Kolmogorov–Smirnov test was performed and all groups were normally distributed. Differences between groups were statistically examined using either a Student's t-test or one-way ANOVA followed by Tukey's post hoc analysis, as stated. $P < 0.05$ was considered significant ($^{*}P \le 0.05$, $^{**}P \le 0.01$, $^{***}P \le 0.001$, $^{****}P \le 0.0001$). The exact *P*-values are provided in Supplementary Table 3.

Reporting summary

Further information on research design is available in the Nature Portfolio Reporting Summary linked to this article.

Data availability

All relevant data supporting the findings of this study are available within the article and its Supplementary Information files or upon request from the corresponding author, Reza Nosrati (reza.nosrati@monash.edu). The data generated in this study are provided in the Source Data file. Source data are provided with this paper.

Code availability

Matlab version 9.7.0.1190202 (R2019b) was used to generate custom scripts based on scripts developed by Ringers et al.[73] to analyse cilia beating and synchronisation. Please contact Reza Nosrati (reza.nosrati@monash.edu) for access.

References

1. Eisenbach, M. & Giojalas, L. C. Sperm guidance in mammals - an unpaved road to the egg. *Nat. Rev. Mol. Cell Biol.* **7**, 276–285 (2006).
2. Fauci, L. J. & Dillon, R. Biofluidmechanics of reproduction. *Annu. Rev. Fluid Mech.* **38**, 371–394 (2006).
3. Nosrati, R. et al. Microfluidics for sperm analysis and selection. *Nat. Rev. Urol.* **14**, 707–730 (2017).
4. Alzamil, L., Nikolakopoulou, K. & Turco, M. Y. Organoid systems to study the human female reproductive tract and pregnancy. *Cell Death Differ.* **28**, 35–51 (2021).
5. Koyama, H., Shi, D. & Fujimori, T. Biophysics in oviduct: planar cell polarity, cilia, epithelial fold and tube morphogenesis, egg dynamics. *Biophys. physicobiology* **16**, 89–107 (2019).
6. Hunter, R. H. F., Coy, P., Gadea, J. & Rath, D. Considerations of viscosity in the preliminaries to mammalian fertilisation. *J. Assist. Reprod. Genet.* **28**, 191–197 (2011).
7. Grudzinskas, J. G., Chapman, M. G., Chard, T. & Djahanbakhch, O. *The Fallopian Tube: Clinical and Surgical Aspects*. (1994).
8. Pillai, V. V., Weber, D. M., Phinney, B. S. & Selvaraj, V. Profiling of proteins secreted in the bovine oviduct reveals diverse functions of this luminal microenvironment. *PLoS One* **12**, 1–22 (2017).
9. Hunter, H. F. R. Modulation of gamete and embryonic microenvironments by oviduct glycoproteins. *Mol. Reprod. Dev.* **39**, 176–181 (1994).
10. Abe, H. The mammalian oviductal epithelium: regional variations in cytological and functional aspects of the oviductal secretory cells. *Histol. Histopathol.* **11**, 743–768 (1996).
11. Leese, H., Tay, J., Reischl, J. & Downing, S. Formation of fallopian tubal fluid: role of a neglected epithelium. *Reproduction* **121**, 339–346 (2001).
12. Hamner, C. E. & Fox, S. B. Effect of oestrogen and progesterone on physical properties of rabbit oviduct fluid. *J. Reprod. Fertil.* **16**, 121–122 (1968).
13. Barton, B. E. et al. Roles of steroid hormones in oviductal function. *Reproduction* **159**, R125–R137 (2020).
14. Raveshi, M. R. et al. Curvature in the reproductive tract alters sperm–surface interactions. *Nat. Commun.* **12**, 3446 (2021).
15. Kress, A. & Morson, G. Changes in the oviducal epithelium during the estrous cycle in the marsupial Monodelphis domestica. *J. Anat.* **211**, 503–517 (2007).
16. Jansen, R. P. S. Fallopian tube isthmic mucus and ovum transport. *Sci. (80-).* **201**, 349–351 (1978).
17. Smith, D. J., Gaffney, E. A., Gadelha, H., Kapur, N. & Kirkman-Brown, J. C. Bend propagation in the flagella of migrating human sperm, and its modulation by viscosity. *Cell Motil. Cytoskeleton* **66**, 220–236 (2009).
18. Pérez-Cerezales, S., López-Cardona, A. P. & Gutiérrez-Adán, A. Progesterone effects on mouse sperm kinetics in conditions of viscosity. *Reproduction* **151**, 501–507 (2016).
19. Miki, K. & Clapham, D. E. Rheotaxis guides mammalian sperm. *Curr. Biol.* **23**, 443–452 (2013).
20. Hyakutake, T., Suzuki, H. & Yamamoto, S. Effect of non-Newtonian fluid properties on bovine sperm motility. *J. Biomech.* **48**, 2941–2947 (2015).
21. Striggow, F. et al. Sperm-driven micromotors moving in oviduct fluid and viscoelastic media. *Small* **16**, e202000213 (2020).
22. Hyakutake, T., Suzuki, H. & Yamamoto, S. Effect of viscosity on motion characteristics of bovine sperm. *J. Aero Aqua Biomechanisms* **4**, 63–70 (2015).
23. Nosrati, R., Driouchi, A., Yip, C. M. M. & Sinton, D. Two-dimensional slither swimming of sperm within a micrometre of a surface. *Nat. Commun.* **6**, 1–9 (2015).
24. Suarez, S. S., Redfern, K., Raynor, P., Martin, F. & Phillips, D. M. Attachment of boar sperm to mucosal explants of oviduct in vitro: Possible role in formation of a sperm reservoir. *Biol. Reprod.* **44**, 998–1004 (1991).
25. Nosrati, R. Lab on a chip devices for fertility: from proof-of-concept to clinical impact. *Lab Chip* **22**, 1680–1689 (2022).

26. Menezo, Y. & Guerin, P. The mammalian oviduct: biochemistry and physiology. *Eur. J. Obstet. Gynecol. Reprod. Biol.* **73**, 99–104 (1997).
27. Jansen, R. P. S. Cyclic changes in the human fallopian tube isthmus and their functional importance. *Am. J. Obstet. Gynecol.* **136**, 292–308 (1980).
28. Hunter, R. H. F. Components of oviduct physiology in eutherian mammals. *Biol. Rev.* **87**, 244–255 (2012).
29. Suarez, S. S. & Dai, X. Hyperactivation enhances mouse sperm capacity for penetrating viscoelastic media. *Biol. Reprod.* **46**, 686–691 (1992).
30. Powar, S. et al. Unraveling the kinematics of sperm motion by reconstructing the flagellar wave motion in 3D. *Small Methods* **6**, 1–10 (2022).
31. Kirkman-Brown, J. C. & Smith, D. J. Sperm motility: is viscosity fundamental to progress? *Mol. Hum. Reprod.* **17**, 539–544 (2011).
32. Saggiorato, G. et al. Human sperm steer with second harmonics of the flagellar beat. *Nat. Commun.* **8**, 1415 (2017).
33. Ishimoto, K., Gadêlha, H., Gaffney, E. A., Smith, D. J. & Kirkman-Brown, J. Human sperm swimming in a high viscosity mucus analogue. *J. Theor. Biol.* **446**, 1–10 (2018).
34. Spassky, N. & Meunier, A. The development and functions of multiciliated epithelia. *Nat. Rev. Mol. Cell Biol.* **18**, 423–436 (2017).
35. Yuan, S. et al. Oviductal motile cilia are essential for oocyte pickup but dispensable for sperm and embryo transport. *Proc. Natl Acad. Sci. USA.* **118**, 1–11 (2021).
36. Ishikawa, T. Axoneme structure from motile cilia. *Cold Spring Harb. Perspect. Biol.* **9**, 1–16 (2017).
37. Gilpin, W., Bull, M. S. & Prakash, M. The multiscale physics of cilia and flagella. *Nat. Rev. Phys.* **2**, 74–88 (2020).
38. Rode, S., Elgeti, J. & Gompper, G. Multi-ciliated microswimmers–metachronal coordination and helical swimming. *Eur. Phys. J. E* **44**, 1–14 (2021).
39. Lyons, R. A., Saridogan, E. & Djahanbakhch, O. The reproductive significance of human Fallopian tube cilia. *Hum. Reprod. Updat.* **12**, 363–372 (2006).
40. Tung, C. K. et al. Microgrooves and fluid flows provide preferential passageways for sperm over pathogen Tritrichomonas foetus. *Proc. Natl Acad. Sci. USA* **112**, 5431–5436 (2015).
41. Beller, F. K., Schumacher, G. F. B., Beier, H. M. & GmbH., O. *The Biology of the Fluids of the Female Genital Tract: Workshop Conference in Murnau, Bavaria, 1979*. (Elsevier North Holland, 1979).
42. Crow, J., Amso, N. N., Lewin, J. & Shaw, R. W. Morphology and ultrastructure of fallopian tube epithelium at different stages of the menstrual cycle and menopause. *Hum. Reprod.* **9**, 2224–2233 (1994).
43. Morales, P., Palma, V., Salgado, A. M. & Villalón, M. Sperm interaction with human oviductal cells in vitro. *Hum. Reprod.* **11**, 1504–1509 (1996).
44. Shnitsar, I. et al. PTEN regulates cilia through Dishevelled. *Nat. Commun.* **6**, 8388 (2015).
45. Karst, A. M. & Drapkin, R. Primary culture and immortalization of human fallopian tube secretory epithelial cells. *Nat. Protoc.* **7**, 1755–1764 (2012).
46. Gargus, E. S., Rogers, H. B., McKinnon, K. E., Edmonds, M. E. & Woodruff, T. K. Engineered reproductive tissues. *Nat. Biomed. Eng.* **4**, 381–393 (2020).
47. Janmohammadi, M. et al. Cellulose-based composite scaffolds for bone tissue engineering and localized drug delivery. *Bioact. Mater.* **20**, 137–163 (2023).
48. Lee, J. et al. Micromechanical property mismatch between pericellular and extracellular matrices regulates stem cell articular and hypertrophic chondrogenesis. *Matter* **6**, 475–492 (2023).
49. Zhang, E. N. et al. Mechanically matched silicone brain implants reduce brain foreign body response. *Adv. Mater. Technol.* **6**, 1–11 (2021).
50. Arora, S., Lin, S., Cheung, C., Yim, E. K. F. & Toh, Y. C. Topography elicits distinct phenotypes and functions in human primary and stem cell derived endothelial cells. *Biomaterials* **234**, 119747 (2020).
51. Gonzalez-Molina, J. et al. Extracellular fluid viscosity enhances liver cancer cell mechanosensing and migration. *Biomaterials* **177**, 113–124 (2018).
52. Bera, K. et al. Extracellular fluid viscosity enhances cell migration and cancer dissemination. *Nature* **611**, 365–373 (2022).
53. Pittman, M. et al. Membrane ruffling is a mechanosensor of extracellular fluid viscosity. *Nat. Phys.* **18**, 1112–1121 (2022).
54. Li, Y., Konstantopoulos, K., Zhao, R., Mori, Y. & Sun, S. X. The importance of water and hydraulic pressure in cell dynamics. *J. Cell Sci.* **133**, jcs240341 (2020).
55. Andrade, Y. N. et al. TRPV4 channel is involved in the coupling of fluid viscosity changes to epithelial ciliary activity. *J. Cell Biol.* **168**, 869–874 (2005).
56. Zaferani, M., Javi, F., Mokhtare, A., Li, P. & Abbaspourrad, A. Rolling controls sperm navigation in response to the dynamic rheological properties of the environment. *Elife* **10**, 1–34 (2021).
57. Eamer, L. et al. Turning the corner in fertility: high DNA integrity of boundary-following sperm. *Lab Chip* **16**, 2418–2422 (2016).
58. Eamer, L., Nosrati, R., Vollmer, M., Zini, A. & Sinton, D. Microfluidic assessment of swimming media for motility-based sperm selection. *Biomicrofluidics* **9**, 044113 (2015).
59. Shamir, E. R. & Ewald, A. J. Three-dimensional organotypic culture: Experimental models of mammalian biology and disease. *Nat. Rev. Mol. Cell Biol.* **15**, 647–664 (2014).
60. Zhang, B., Korolj, A., Lai, B. F. L. & Radisic, M. Advances in organ-on-a-chip engineering. *Nat. Rev. Mater.* **3**, 257–278 (2018).
61. Young, R. E. & Huh, D. D. Organ-on-a-chip technology for the study of the female reproductive system. *Adv. Drug Deliv. Rev.* **173**, 461–478 (2021).
62. Kawakita, S. et al. Organ-on-a-chip models of the blood–brain barrier: recent advances and future prospects. *Small* **18**, e2201401 (2022).
63. Humayun, M., Chow, C. W. & Young, E. W. K. Microfluidic lung airway-on-a-chip with arrayable suspended gels for studying epithelial and smooth muscle cell interactions. *Lab Chip* **18**, 1298–1309 (2018).
64. Xiao, S. et al. A microfluidic culture model of the human reproductive tract and 28-day menstrual cycle. *Nat. Commun.* **8**, 14584 (2017).
65. Ferraz, M. A. M. M. et al. Improved bovine embryo production in an oviduct-on-a-chip system: prevention of poly-spermic fertilization and parthenogenic activation. *Lab Chip* **17**, 905–916 (2017).
66. Ferraz, M. A. M. M. et al. An oviduct-on-a-chip provides an enhanced in vitro environment for zygote genome reprogramming. *Nat. Commun.* **9**, 4934 (2018).
67. Fotheringham, S., Levanon, K. & Drapkin, R. Ex vivo culture of primary human fallopian tube epithelial cells. *J. Vis. Exp.* **51**, e2728 (2011).
68. Lavanya, M. et al. Microenvironment of the male and female reproductive tracts regulate sperm fertility: impact of viscosity, pH, and osmolality. *Andrology* **10**, 92–104 (2022).
69. Utsunomiya, T. et al. Creation, effects on embryo quality, and clinical outcomes of a new embryo culture medium with 31 optimized components derived from human oviduct fluid: a prospective multicenter randomized trial. *Reprod. Med. Biol.* **21**, 1–12 (2022).
70. Moghissi, K. S. Human fallopian tube fluid. i. protein composition. *Fertil. Steril.* **21**, 821–829 (1970).
71. Zhu, M., Iwano, T. & Takeda, S. Fallopian tube basal stem cells reproducing the epithelial sheets in vitro—stem cell of fallopian epithelium. *Biomolecules* **10**, 1–15 (2020).

72. Satir, P. & Sleigh, M. A. The physiology of cilia and mucociliary interactions. *Annu. Rev. Physiol.* **52**, 137–155 (1990).
73. Ringers, C. et al. Novel analytical tools reveal that local synchronization of cilia coincides with tissue-scale metachronal waves in zebrafish multiciliated epithelia. *Elife* **12**, 1–27 (2023).
74. Khaderi, S. N., Den Toonder, J. M. J. & Onck, P. R. Microfluidic propulsion by the metachronal beating of magnetic artificial cilia: A numerical analysis. *J. Fluid Mech.* **688**, 44–65 (2011).
75. Milana, E. et al. Metachronal patterns in artificial cilia for low Reynolds number fluid propulsion. *Sci. Adv.* **6**, 1–8 (2020).
76. Brumley, D. R., Polin, M., Pedley, T. J. & Goldstein, R. E. Hydrodynamic synchronization and metachronal waves on the surface of the colonial alga Volvox carteri. *Phys. Rev. Lett.* **109**, 28–32 (2012).
77. Lorenzo, I. M., Liedtke, W., Sanderson, M. J. & Valverde, M. A. TRPV4 channel participates in receptor-operated calcium entry and ciliary beat frequency regulation in mouse airway epithelial cells. *Proc. Natl Acad. Sci. USA* **105**, 12611–12616 (2008).
78. Liedtke, W. et al. Vanilloid receptor-related osmotically activated channel (VR-OAC), a candidate vertebrate osmoreceptor. *Cell* **103**, 525–535 (2000).
79. Liedtke, W., Tobin, D. M., Bargmann, C. I. & Friedman, J. M. Mammalian TRPV4 (VR-OAC) directs behavioral responses to osmotic and mechanical stimuli in Caenorhabditis elegans. *Proc. Natl Acad. Sci. USA* **100**, 14531–14536 (2003).
80. Moreau, B., Nelson, C. & Parekh, A. B. Biphasic Regulation of Mitochondrial Ca2+ Uptake by Cytosolic Ca2+ Concentration. *Curr. Biol.* **16**, 1672–1677 (2006).
81. Williams, G. S. B., Boyman, L., Chikando, A. C., Khairallah, R. J. & Lederer, W. J. Mitochondrial calcium uptake. *Proc. Natl Acad. Sci. USA* **110**, 10479–10486 (2013).
82. Van Blerkom, J., Davis, P. & Alexander, S. Inner mitochondrial membrane potential (ΔΨm), cytoplasmic ATP content and free Ca2+ levels in metaphase II mouse oocytes. *Hum. Reprod.* **18**, 2429–2440 (2003).
83. McKenzie, M., Lim, S. C. & Duchen, M. R. Simultaneous measurement of mitochondrial calcium and mitochondrial membrane potential in live cells by fluorescent microscopy. *J. Vis. Exp.* **2017**, 2–7 (2017).
84. Jouaville, L. S., Pinton, P., Bastianutto, C., Rutter, G. A. & Rizzuto, R. Regulation of mitochondrial ATP synthesis by calcium: Evidence for a long-term metabolic priming. *Proc. Natl Acad. Sci. USA* **96**, 13807–13812 (1999).
85. Tarasov, A. I., Griffiths, E. J. & Rutter, G. A. Regulation of ATP production by mitochondrial Ca2+. *Cell Calcium* **52**, 28–35 (2012).
86. Kim, B., Lee, H., Kawata, K. & Park, J. Y. Exercise-mediated wall shear stress increases mitochondrial biogenesis in vascular endothelium. *PLoS One* **9**, e111409 (2014).
87. Bavli, D. et al. Real-time monitoring of metabolic function in liver-on-chip microdevices tracks the dynamics of Mitochondrial dysfunction. *Proc. Natl Acad. Sci. USA* **113**, E2231–E2240 (2016).
88. Zhou, R., Yazdi, A. S., Menu, P. & Tschopp, J. A role for mitochondria in NLRP3 inflammasome activation. *Nature* **469**, 221–226 (2011).
89. Khatib, N. S. et al. Mechanoregulatory role of TRPV4 in prenatal skeletal development. *Sci. Adv.* **9**, 1–18 (2023).
90. Baratchi, S. et al. Shear stress mediates exocytosis of functional TRPV4 channels in endothelial cells. *Cell. Mol. Life Sci.* **73**, 649–666 (2016).
91. Derouiche, S., Takayama, Y., Murakami, M. & Tominaga, M. TRPV4 heats up ANO1-dependent exocrine gland fluid secretion. *FASEB J.* **32**, 1841–1854 (2018).
92. Reiter, B. et al. TRPV4-mediated regulation of epithelial permeability. *FASEB J.* **20**, 1802–1812 (2006).
93. Nadezhdin, K. D. et al. Structure of human TRPV4 in complex with GTPase RhoA. *Nat. Commun.* **14**, 3733 (2023).
94. Button, B. et al. A periciliary brush promotes the lung health by separating the mucus layer from airway epithelia. *Sci. (80-).* **337**, 937–941 (2012).
95. Donnez, J., Casanas-Roux, F., Caprasse, J., Ferin, J. & Thomas, K. Cyclic changes in ciliation, cell height, and mitotic activity in human tubal epithelium during reproductive life. *Fertil. Steril.* **43**, 554–559 (1985).
96. Kessler, M. et al. The Notch and Wnt pathways regulate stemness and differentiation in human fallopian tube organoids. *Nat. Commun.* **6**, 8989 (2015).
97. Totaro, A., Castellan, M., Di Biagio, D. & Piccolo, S. Crosstalk between YAP/TAZ and Notch Signaling. *Trends Cell Biol.* **28**, 560–573 (2018).
98. Totaro, A. et al. YAP/TAZ link cell mechanics to Notch signalling to control epidermal stem cell fate. *Nat. Commun.* **8**, 1–13 (2017).
99. Engel-Pizcueta, C. & Pujades, C. Interplay between notch and YAP/TAZ pathways in the regulation of cell fate during embryo development. *Front. Cell Dev. Biol.* **9**, 1–13 (2021).
100. Dupont, S. et al. Role of YAP/TAZ in mechanotransduction. *Nature* **474**, 179–184 (2011).
101. Cancer, T. & Atlas, G. Integrated genomic analyses of ovarian carcinoma. *Nature* **474**, 609–615 (2011).
102. O'Callaghan, C. L., Sikand, K., Rutman, A. & Hirst, R. A. The effect of viscous loading on brain ependymal cilia. *Neurosci. Lett.* **439**, 56–60 (2008).
103. Chen, D. T. N., Heymann, M., Fraden, S., Nicastro, D. & Dogic, Z. ATP consumption of eukaryotic flagella measured at a single-cell level. *Biophys. J.* **109**, 2562–2573 (2015).
104. Hill, D. B. et al. Force generation and dynamics of individual cilia under external loading. *Biophys. J.* **98**, 57–66 (2010).
105. Yazdan Parast, F. et al. Viscous loading regulates the flagellar energetics of human and bull sperm. *Small Methods* **2300928**, 1–12 (2023).
106. Chakrabarti, B., Fürthauer, S. & Shelley, M. J. A multiscale biophysical model gives quantized metachronal waves in a lattice of beating cilia. *Proc. Natl Acad. Sci. USA* **119**, 1–13 (2022).
107. Marshall, W. et al. Multi-scale spatial heterogeneity enhances particle clearance in airway ciliary arrays. *Nat. Phys.* **16**, 958–964 (2020).
108. Feriani, L. et al. Assessing the collective dynamics of motile cilia in cultures of human airway cells by multiscale DDM. *Biophys. J.* **113**, 109–119 (2017).
109. Sanderson, M. J. & Sleigh, M. A. Ciliary activity of cultured rabbit tracheal epithelium: beat pattern and metachrony. *J. Cell Sci.* **47**, 331–347 (1981).
110. Suarez, S. S. Mammalian sperm interactions with the female reproductive tract. *Cell Tissue Res.* **363**, 185–194 (2016).
111. Hartman, C. G. How large is the mammalian egg?: a review. *Q. Rev. Biol.* **4**, 373–388 (1929).
112. Lyons, R. A. et al. Fallopian tube ciliary beat frequency in relation to the stage of menstrual cycle and anatomical site. *Hum. Reprod.* **17**, 584–588 (2002).
113. Sharma, S., Goswami, R., Zhang, D. X. & Rahaman, S. O. TRPV4 regulates matrix stiffness and TGFβ1-induced epithelial-mesenchymal transition. *J. Cell. Mol. Med.* **23**, 761–774 (2019).
114. Kanugula, A. K. et al. Novel noncanonical regulation of soluble VEGF/VEGFR2 signaling by mechanosensitive ion channel TRPV4. *FASEB J.* **33**, 195–203 (2019).
115. Batan, D. et al. Hydrogel cultures reveal transient receptor potential vanilloid 4 regulation of myofibroblast activation and proliferation in valvular interstitial cells. *FASEB J.* **36**, 1–16 (2022).
116. De Clercq, K. et al. Functional expression of transient receptor potential channels in human endometrial stromal cells during the luteal phase of the menstrual cycle. *Hum. Reprod.* **30**, 1421–1436 (2015).

117. Jung, C. et al. The progesterone receptor regulates the expression of TRPV4 channel. *Pflug. Arch. Eur. J. Physiol.* **459**, 105–113 (2009).
118. Slayden, O. D., Luo, F. & Bishop, C. V. Physiological action of progesterone in the nonhuman primate oviduct. *Cells* **11**, 1534 (2022).
119. Winters, S. L., Davis, C. W. & Boucher, R. C. Mechanosensitivity of mouse tracheal ciliary beat frequency: roles for Ca2+, purinergic signaling, tonicity, and viscosity. *Am. J. Physiol. - Lung Cell. Mol. Physiol.* **292**, 614–624 (2007).
120. Nakahari, T. Regulation of ciliary beat frequency in airways: shear stress, ATP action, and its modulation. *Am. J. Physiol. - Lung Cell. Mol. Physiol.* **292**, 612–613 (2007).
121. Acevedo, C., Blanchard, K., Bacigalupo, J. & Vergara, C. Possible ATP trafficking by ATP-shuttles in the olfactory cilia and glucose transfer across the olfactory mucosa. *FEBS Lett.* **593**, 601–610 (2019).
122. Noguchi, M., Sawada, T. & Akazawa, T. ATP-regenerating system in the cilia of Paramecium caudatum. *J. Exp. Biol.* **204**, 1063–1071 (2001).
123. Suarez, S. S. & Pacey, A. A. Sperm transport in the female reproductive tract. *Hum. Reprod. Update* **12**, 23–37 (2006).
124. Leung, E. T. Y. et al. Simulating nature in sperm selection for assisted reproduction. *Nat. Rev. Urol.* **19**, 16–36 (2022).
125. Ertan Kervancioglu, M., Saridogan, E., John Aitken, R. & Djahanbakhch, O. Importance of sperm-to-epithelial cell contact for the capacitation of human spermatozoa in fallopian tube epithelial cell cocultures. *Fertil. Steril.* **74**, 780–784 (2000).
126. Roest, I. et al. What is the fertility-enhancing effect of tubal flushing? a hypothesis article. *J. Obstet. Gynaecol. (Lahore).* **42**, 1619–1625 (2022).
127. Baratchi, S. et al. The TRPV4 agonist GSK1016790A regulates the membrane expression of TRPV4 channels. *Front. Pharmacol.* **9**, 1–12 (2019).
128. Lamandé, S. R. et al. Mutations in TRPV4 cause an inherited arthropathy of hands and feet. *Nat. Genet.* **43**, 1142–1146 (2011).
129. Martínez-Rendón, J. et al. TRPV4 regulates tight junctions and affects differentiation in a cell culture model of the corneal epithelium. *J. Cell. Physiol.* **232**, 1794–1807 (2017).
130. Lee, H. pyo, Stowers, R. & Chaudhuri, O. Volume expansion and TRPV4 activation regulate stem cell fate in three-dimensional microenvironments. *Nat. Commun.* **10**, 529 (2019).
131. Siroky, B. J. et al. Primary cilia regulate the osmotic stress response of renal epithelial cells through TRPM3. *Am. J. Physiol. - Ren. Physiol.* **312**, F791–F805 (2017).

Acknowledgements

This work was supported by the Australian Research Council (ARC) Discovery Project Grants (DP190100343), the Australian National Health and Medical Research Council (NHMRC) fellowship (Investigator Grant 2017370) to R.N., and Monash University (Faculty of Engineering) Postgraduate Publications Award (PPA) to M.S.A.H. The authors acknowledge the use of facilities at Monash Micro Imaging Centre, Clayton. The authors also thank Wagstaff, Cranbourne, for their assistance in providing the ewe oviduct samples.

Author contributions

M.S.A.H. and R.N. designed the research. M.S.A.H. and J.M.D. performed research. M.S.A.H., J.M.D., M.M.G, M.K.O., and R.N. analysed data and wrote the paper.

Competing interests

The authors declare no competing interests.

Additional information

Supplementary information The online version contains supplementary material available at https://doi.org/10.1038/s41467-024-51481-9.

Correspondence and requests for materials should be addressed to Reza Nosrati.

Peer review information *Nature Communications* thanks Bart Gadella, Annie Viallat and the other, anonymous, reviewer for their contribution to the peer review of this work. A peer review file is available.